
Unifying Text Semantics and Graph Structures for Temporal Text-attributed Graphs with Large Language Models

Siwei Zhang¹ Yun Xiong¹ Yateng Tang² Xi Chen¹ Zian Jia¹ Zehao Gu¹ Jiarong Xu¹ Jiawei Zhang³

Abstract

Temporal graph neural networks (TGNNs) have shown remarkable performance in temporal graph modeling. However, real-world temporal graphs often possess rich textual information, giving rise to temporal text-attributed graphs (TTAGs). Such combination of dynamic text semantics and evolving graph structures introduces heightened complexity. Existing TGNNs embed texts statically and rely heavily on encoding mechanisms that biasedly prioritize structural information, overlooking the temporal evolution of text semantics and the essential interplay between semantics and structures for synergistic reinforcement. To tackle these issues, we present **CROSS**, a novel framework that seamlessly extends existing TGNNs for TTAG modeling. The key idea is to employ the advanced large language models (LLMs) to extract the dynamic semantics in text space and then generate expressive representations unifying both semantics and structures. Specifically, we propose a Temporal Semantics Extractor in the CROSS framework, which empowers the LLM to offer the temporal semantic understanding of node’s evolving contexts of textual neighborhoods, facilitating semantic dynamics. Subsequently, we introduce the Semantic-structural Co-encoder, which collaborates with the above Extractor for synthesizing illuminating representations by jointly considering both semantic and structural information while encouraging their mutual reinforcement. Extensive experimental results on four public datasets and one practical industrial dataset demonstrate CROSS’s significant effectiveness and robustness.

1. Introduction

Temporal graphs are crucial for modeling dynamic interaction data, where objects are represented as nodes and timestamped interactions are depicted as edges (Zhang et al., 2023). Unlike static graphs, temporal graphs continuously evolve over time. To capture temporal dependencies and realize representation learning for such graphs, extensive research has developed temporal graph neural networks (TGNNs) (Yu et al., 2023; Huang et al., 2024). These works typically adopt structural encoding mechanisms (Zhang et al., 2024b) to encapsulate the dynamics of graph structures, thus enabling representations for downstream tasks.

Meanwhile, besides the dynamically evolving graph structures, real-world temporal graphs are also often accompanied by rich text attributes, giving rise to temporal text-attributed graphs (TTAGs) (Zhang et al., 2024a). As shown in Fig. 1(a), in e-commerce networks, nodes may encompass elaborate text descriptions such as user profile or product introduction, while edges can attach transaction details including price, transaction type, review, *etc.* Representation learning in TTAGs presents unique challenges due to the intricate combination of dynamic text semantics and evolving graph structures, which remains largely unexplored within the community. Despite the notable success of existing TGNNs, they still encounter two fundamental limitations that hinder their accommodation to TTAG modeling.

Neglect of semantic dynamics. Text semantics arise from the textual attributes of a node and its surrounding neighborhoods. These semantics exhibit changes across timestamps due to the temporal evolution of neighborhood contexts in TTAGs. For example, as depicted in Fig. 1(a), the term “*apple*” may take on different meanings according to user preferences (driven by its neighborhoods), such as “*smartphone*” when focused on technology while “*fruit*” when turning to daily life. Such characteristics necessitate a temporal-aware design for extracting text semantics over time. However, existing TGNNs always use pre-trained language models, *e.g.*, MiniLM (Wang et al., 2020), to statically embed texts as pre-processed features, failing to adapt to such dynamic semantic shifts and leading to suboptimal representations for effectively capturing the semantic dynamics.

Ineffective semantic-structural reinforcement modeling. Another limitation of existing TGNNs is the rigid reliance

*Equal contribution ¹Shanghai Key Laboratory of Data Science, School of Computer Science, Fudan University ²Wechat Pay, Tencent Group ³IFM Lab, Department of Computer Science, University of California, Davis. Correspondence to: Siwei Zhang <swzhang24@m.fudan.edu.cn>.

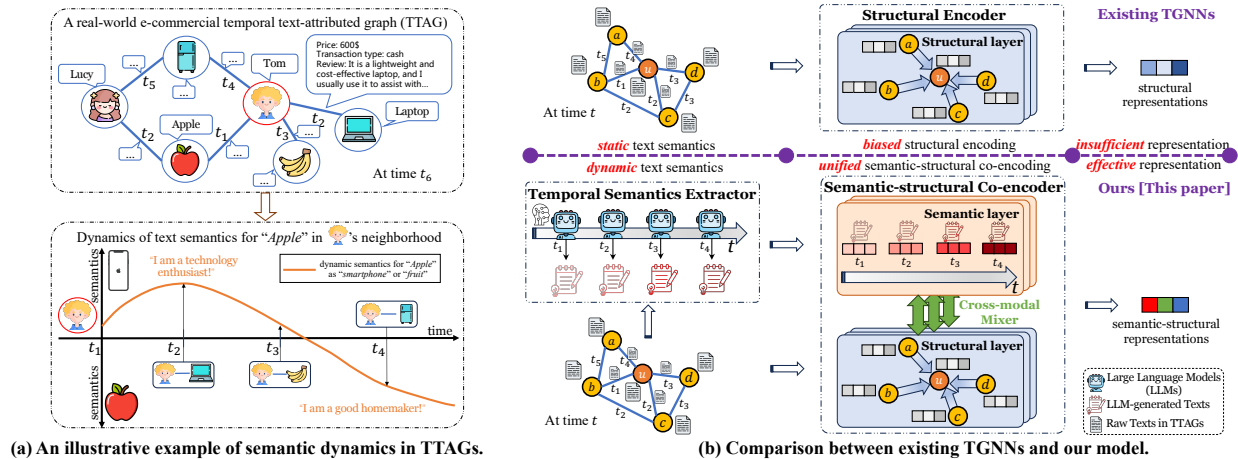


Figure 1. (a) Temporal text-attributed graphs (TTAGs) naturally exhibit semantic dynamics, where text semantics around nodes dynamically evolve across temporal dimensions. (b) Different from existing TGNNs that biasedly focus on structural information, our model seamlessly unifies text semantics and graph structures, promoting both dynamic semantic understanding and semantic-structural reinforcement.

on their structural encoding mechanisms, which predominantly focus on topological information without adequately incorporating semantic considerations. We argue that the semantics and structures within TTAGs can mutually reinforce each other, making a biased encoding mechanism that solely emphasizes structures untenable. This hypothesis is reasonable due to the inherent interplay between textual content and structural connectivity (Zou et al., 2021). For instance, product recommendations are shaped not only by goods’ descriptions but also by users’ historical behaviors (Ren et al., 2024). Existing encoding mechanisms of TGNNs do not account for such nuanced semantic-structural reinforcement in TTAGs, resulting in insufficient representations overly reliant on simplistic (sometimes noisy) structural information.

On the other hand, large language models (LLMs) (Fang et al., 2024) have revolutionized the field of graph semantic modeling. Recent works (Chen et al., 2024b; Tang et al., 2024) reveal that LLMs, e.g., DeepSeek-v2/3 (Liu et al., 2024), exhibit exceptional natural language understanding and generation abilities, which have greatly enhanced graph modeling via various techniques like text augmentation (He et al., 2023) or structure refinement (Li et al., 2024). Such impressive semantic expertise inspires us to harness LLMs as a promising solution to the aforementioned limitations of existing TGNNs. Consequently, the key idea of this work is to leverage the outstanding capabilities of LLMs to explicitly extract dynamic semantics in text space, which subsequently allows for a non-biased, unified, and integrated encoding mechanism obeying semantic-structural reinforcement.

In this paper, we aim to extend existing TGNNs for TTAG modeling by adeptly capturing semantic dynamics and promoting semantic-structural reinforcement during the encoding process as illustrated in Fig. 1(b). We introduce **CROSS** (Cohesive Representation Of Semantics and Structures), a novel TGNN-agnostic framework that seamlessly integrates

both text semantics and graph structures with the help of LLMs. CROSS can significantly boost existing TGNNs, and it comprises two main components: (i) Temporal Semantics Extractor, and (ii) Semantic-structural Co-encoder. To capture the temporal semantics for nodes within TTAGs, we propose a Temporal Semantics Extractor, which enables the LLM to dynamically derive the temporal semantic understanding for the evolving contexts of nodes’ neighborhoods. It automatically detects semantic dynamics by constructing a temporal reasoning chain to sequentially prompt the LLM to summarize the nodes’ textualized neighborhoods, thus revealing the linguistic nuances across temporal dimensions. Besides the Extractor, to effectively achieve semantic-structural reinforcement, we further propose the Semantic-structural Co-encoder that simultaneously exploits both semantic and structural information through an iterative, multi-layer design. Each layer in the proposed Co-encoder bidirectionally transfers the cross-modal information between semantics and structures, allowing both modalities to blend deeply and fully illuminate each other. By performing such unified integration, we can generate effective representations that are both semantic-enriched and structural-informed.

In summary, the main contributions of this paper include:

- We focus on an unexplored problem of temporal text-attributed graph (TTAG) modeling. To address this problem, we introduce CROSS that flexibly boosts the capability of existing TGNNs for adapting to TTAG modeling.
- We develop a Temporal Semantics Extractor, which allows the LLM to dynamically provide the temporal semantic understanding for nodes’ neighborhoods, effectively detecting semantic dynamics.
- We propose a Semantic-structural Co-encoder that jointly propagates semantic and structural information, facilitating mutual reinforcement between both modalities.
- We conduct extensive experiments on four public datasets

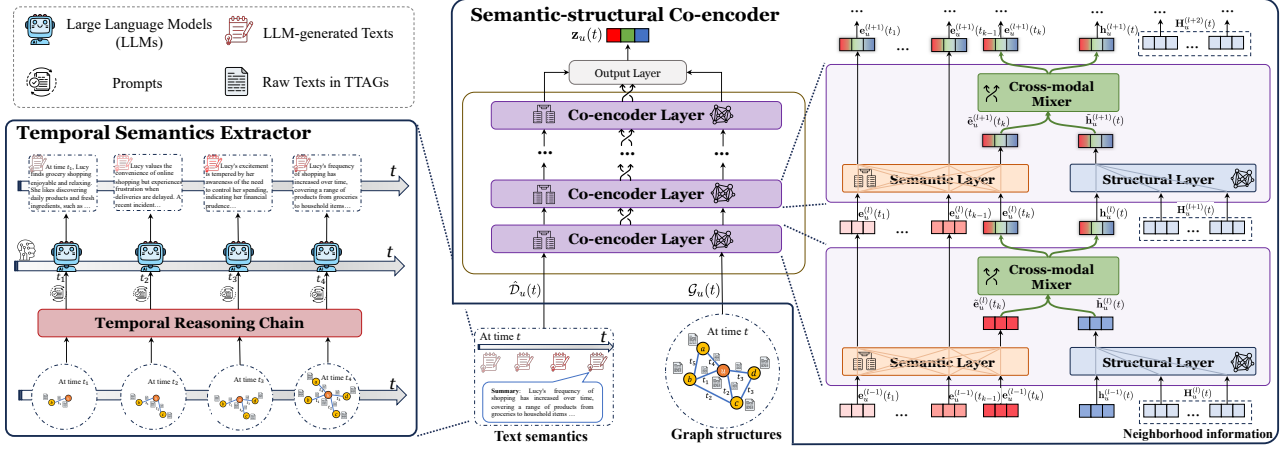


Figure 2. Framework of the proposed model. Our Temporal Semantics Extractor constructs the temporal reasoning chain to empower the LLM to dynamically provide the semantic understanding of nodes’ neighborhoods along temporal dimensions, thereby explicitly extracting semantic dynamics in text space. Subsequently, the Semantic-structural Co-encoder iteratively mixes and consolidates both semantic and structural information, ensuring their mutual reinforcement for effectively generating more expressive representations.

and one practical e-commercial industrial dataset. CROSS outperforms baselines by 24.7% on average in temporal link prediction and 3.7% in an industrial application.

2. Terminology Preliminaries

Definition 1. Temporal Text-attributed Graph. Given a set of nodes \mathcal{V} , node text attributes \mathcal{D} , and edge text attributes \mathcal{R} , a temporal text-attributed graph can be represented as a sequence of interactions $\mathcal{G} = \{(u, v, t)\}$, where $u, v \in \mathcal{V}$ and $t \geq 0$. Each node $u \in \mathcal{V}$ is associated with a node text attribute $d_u \in \mathcal{D}$ and each interaction $(u, v, t) \in \mathcal{G}$ attaches an edge text attribute $r_{u,v,t} \in \mathcal{R}$. We use $\mathcal{H}_u(t) = \{(u, v, \tau) | \tau < t\} \cup \{(v, u, \tau) | \tau < t\}$ to denote the set of historical interactions involving node u before time t .

Definition 2. Temporal Text-attributed Graph Modeling. Given node u , time t , and all available historical interactions before t , $\{(u', v', \tau) | \tau < t\}$, temporal text-attributed graph modeling aims to learn a mapping function $f : (u, t) \mapsto \mathbf{z}_u(t)$, where $\mathbf{z}_u(t) \in \mathbb{R}^d$ denotes the representation of node u at time t , and d is the vector dimension.

Definition 3. Language Model vs Large Language Model. We clearly distinguish between pre-trained language models (LMs) and large language models (LLMs). LMs, such as MiniLM, are relatively smaller models designed to embed texts from the text space into the feature space; and LLMs refer to significantly larger models far surpassing the linguistic capabilities of LMs, like DeepSeek-v2/3.

3. Methodology

As mentioned before, TTAG modeling requires considering both semantic dynamics and semantic-structural reinforcement. To this end, as depicted in Fig. 2, the proposed CROSS framework comprises two stages, *i.e.*, the Temporal Semantics Extractor first detects the dynamic text seman-

tics for nodes’ evolving neighborhoods; then the Semantic-structural Co-encoder jointly unifies both semantic and structural information to ensure cross-modal reinforcement. We will introduce these two stages in the following subsections.

3.1. Temporal Semantics Extractor

The dynamics of graph structures within TTAGs makes summarizing nodes’ textual contexts more challenging. Existing methods (He et al., 2023) that leverage LLMs for external knowledge summarization primarily focus on static text-attributed graphs. They typically adopt indiscriminate, one-time reasoning for each node solely based on its own text attribute. Such methods may be suboptimal for TTAGs as they fail to capture the contextual evolution of these graphs, where nodes’ textural neighborhoods dynamically change over time. To address this challenge, we strategically design a novel temporal reasoning chain that empowers LLMs with the dynamic semantic summarization reasoning capability along temporal dimensions, effectively discerning the evolving linguistic nuances within neighborhood contexts.

Temporal Reasoning Chain. Now, we introduce the temporal reasoning chain that facilitates LLMs to dynamically summarize nodes’ neighborhoods along timestamps. However, performing LLM reasoning at every timestamp is computationally prohibitive and impractical. Therefore, to constrain the reasoning steps for nodes while ensuring that each LLM reasoning can access a stable and balanced number of interactions, we thoughtfully sample reasoning timestamps at equal interaction intervals, striking a delicate balance between temporal granularity and computational efficiency.

Formally, for node u , we first derive the set of its interaction timestamps $\mathcal{T}_u = \{t_1, t_2, \dots, t_n\}$, where $t_1 \leq t_2 \leq \dots \leq t_n$ and n is the node degree. Then we sample the reasoning timestamps at intervals of $\lceil \frac{n}{m} \rceil$ among \mathcal{T}_u with a predefined maximum reasoning count m for each node as follows:

$$\hat{\mathcal{T}}_u = \left\{ \hat{t}_i \mid \hat{t}_i = \begin{cases} t_{i \cdot \lceil \frac{n}{m} \rceil}, & i = 1, \dots, m-1, \\ t_n, & i = m \end{cases} \in \mathcal{T}_u \right\}. \quad (1)$$

Here, $\hat{\mathcal{T}}_u \subseteq \mathcal{T}_u$ depicts the LLM reasoning timestamps to summarize text semantics around node u , and we will also analyze the dataset-specific hyper-parameter m in Sec. 4.6.

LLM Summarization. Since the graph models may struggle to effectively incorporate textual rationales (Tan et al., 2024), we employ the powerful LLM to explicitly capture semantic dynamics for nodes’ neighborhoods. Specifically, we perform multi-turn calling with LLM for each node in the order of the previously sampled reasoning timestamps. Given node u at each reasoning time $\hat{t} \in \hat{\mathcal{T}}_u$, we first obtain its neighborhood by retrieving u ’s historical interactions $\mathcal{H}_u(\hat{t}) = \{(u, v, \tau) \mid \tau < \hat{t}\} \cup \{(v, u, \tau) \mid \tau < \hat{t}\}$, and then we prompt the LLM to generate neighborhood summaries and semantic details, which can be represented by:

$$\hat{d}_u(\hat{t}) = \text{LLM}\left(d_u, \hat{t}, \{r_*\}_{* \in \mathcal{H}_u(\hat{t})}; \text{PROMPT}\right). \quad (2)$$

$\text{LLM}(\cdot; \text{PROMPT})$ denotes the LLM calling with the prompt, which comprises a fixed template alongside variable pieces, including node u ’s raw text attribute d_u , time \hat{t} , and the textual neighborhood $\{r_*\}_{* \in \mathcal{H}_u(\hat{t})}$. $\hat{d}_u(\hat{t})$ is the LLM-generated text, denoting the provided summary in response. We present a simplified example of PROMPT for clarity, and the complete version is also given in Sec. G of the Appendix.

A simplified example of PROMPT

Goal: [Request to summarize the current neighborhoods and emphasize the response format.]
Descriptions: [Provide the node text attribute d_u .]
Current time: [Specify the reasoning time \hat{t} .]
Historical interactions: [List the textualized neighborhoods using recent interactions $\{r_*\}_{* \in \mathcal{H}_u(\hat{t})}$.]

After performing all reasoning, we can obtain the set of LLM-generated textual summaries for each node u . We represent them as $\hat{\mathcal{D}}_u = \{\hat{d}_u(\hat{t}) \mid \hat{t} \in \hat{\mathcal{T}}_u\}$. Notably, to incorporate the raw texts in TTAGs, we set $\hat{d}_u(0) = d_u$. These textual summaries encapsulate the text semantics surrounding each node across timestamps using the advanced capabilities of the LLM, effectively promoting semantic dynamics within the text space for TTAG modeling.

3.2. Semantic-structural Co-encoder

As mentioned in the Introduction, existing TGNNs solely account for structural information during encoding, overlooking the necessary consideration of dynamic semantic insights and the reinforcement between both modalities. To address this issue, our Semantic-structural Co-encoder performs iterative integration of semantics and structures at the

layer level. Each layer of the proposed Co-encoder comprises three types of encoding components: (i) a semantic layer that encodes the text semantics from LLM-generated summaries to produce semantic representations; (ii) a structural layer that encodes the graph structures from neighborhood information to capture structural representations; and (iii) a cross-modal mixer that facilitates transformation between these two unimodal representations to cheer their mutual reinforcement. We will discuss them in detail below.

Semantic Layer. We implement the semantic layer using a Transformer encoder (Vaswani et al., 2017) due to its strong alignment with textual modality and its widespread usage in semantic modeling. It can take any form as long as efficient.

We first prepare the inputs for the semantic layer. For node u at time t , the inputs of the semantic layer are the corresponding LLM-generated summaries before t from our Extractor. We represent them as $\hat{\mathcal{D}}_u(t) = \{\hat{d}_u(t_k) \mid t_k < t\}$, where $t_1 \leq \dots \leq t_k$. We then use a pre-trained LM, such as MiniLM (Wang et al., 2020), to embed the texts into the d -dimensional semantic features, which is depicted as $\hat{s}_u(t_k) = \text{LM}(\hat{d}_u(t_k)) \in \mathbb{R}^d$. To capture the temporal differences, we subsequently concatenate time information into these semantic features as follows:

$$\mathbf{x}_u(t_k) = \hat{s}_u(t_k) \parallel \Phi(t - t_k) \in \mathbb{R}^{2d}. \quad (3)$$

$\Phi(\cdot)$ is the time encoding function introduced by (Kazemi et al., 2019), which is widely used in recent TGNNs.

These enriched features then feed into the L -layer Transformer encoder blocks to compute the semantic representations for node u at time t . We have:

$$\tilde{\mathbf{e}}_u^{(l)}(t_1), \dots, \tilde{\mathbf{e}}_u^{(l)}(t_k) = \text{TRM}^{(l)}\left(\mathbf{e}_u^{(l-1)}(t_1), \dots, \mathbf{e}_u^{(l-1)}(t_k)\right), \quad (4)$$

where $\tilde{\mathbf{e}}_u^{(l)}(t) \in \mathbb{R}^{2d}$ corresponds to the pre-mixed semantic representation at the l -th layer and $\mathbf{e}_u^{(0)}(t_1), \dots, \mathbf{e}_u^{(0)}(t_k) = \mathbf{x}_u(t_1), \dots, \mathbf{x}_u(t_k)$. As we will mention below, the latest semantic representation of node u , $\mathbf{e}_u^{(l-1)}(t_k)$, has integrated information from its structural representation in the previous layer. This allows the l -th semantic layer to receive the information from graph structures, achieving deep fusion and promoting their synergistic reinforcement.

Structural Layer. Meanwhile, we conduct the structural layer to encode the graph structures around node u at time t , $\mathcal{G}_u(t)$, using the structural encoding block in TGNNs.

Formally, the l -th structural layer aggregates the neighborhood information of node u in current layer $\mathbf{H}_u^{(l)}(t)$ and its structural representation from the previous layer $\mathbf{h}_u^{(l-1)}(t)$ with a 2-layer Multi-Layer Perceptron (MLP):

$$\tilde{\mathbf{h}}_u^{(l)}(t) = \text{MLP}^{(l)}\left(\mathbf{h}_u^{(l-1)}(t) \parallel \text{AGG}\left(\mathbf{H}_u^{(l)}(t)\right)\right). \quad (5)$$

Here, $\tilde{\mathbf{h}}_u^{(l)}(t)$ is the pre-mixed structural representation at the l -th layer and \parallel denotes concatenation. $\text{AGG}(\cdot)$ is a pooling function to aggregate the neighborhood information matrix into a d -dimensional vector, with specific implementations (e.g., mean, sum) varying across various TGNNs.

The neighborhood information $\mathbf{H}_u^{(l)}(t)$ is derived using a temporal attention mechanism (Xu et al., 2020) via message passing from the l -th layer neighborhood. This process assigns attention weights to scale the contribution and importance of neighbors $\mathcal{N}_u(t)$ for node u as follows:

$$\mathbf{H}_u^{(l)}(t) = \text{SOFTMAX}(\mathbf{a}_u^{(l)}(t)) \cdot \mathbf{V}_u^{(l)}(t), \quad (6)$$

where $\mathbf{a}_u^{(l)}(t) = [a_{uv}^{(l)}(t)]_{v \in \mathcal{N}_u(t)}$ represents the attention weight vector, and the matrix $\mathbf{V}_u^{(l)}(t) = [\mathbf{v}_v^{(l)}(t)]_{v \in \mathcal{N}_u(t)}$ condenses the messages from u 's l -th layer neighborhood.

Each element $a_{uv}^{(l)}(t)$ in $\mathbf{a}_u^{(l)}(t)$ is the importance weight for node u to its neighbor $v \in \mathcal{N}_u(t)$, which is computed as:

$$a_{uv}^{(l)}(t) = \frac{f_q(\mathbf{h}_u^{(l-1)}(t)) f_k(\mathbf{h}_v^{(l-1)}(t))^T}{\sqrt{d^{(k)}}}; \quad (7)$$

and each row $\mathbf{v}_v^{(l)}(t)$ from $\mathbf{V}_u^{(l)}(t)$ is the message carried from u 's neighboring node v , which is determined by:

$$\mathbf{v}_v^{(l)}(t) = f_v(\mathbf{h}_v^{(l-1)}(t)). \quad (8)$$

In Eqs. 7 & 8, $f_*(\cdot)$ ($* \in \{q, k, v\}$) denote the encoding functions for queries, keys, and values, respectively (Vaswani et al., 2017). These functions may be implemented differently across various TGNNs (Xu et al., 2020; Rossi et al., 2020a; Yu et al., 2023), and we do not discuss their details as they are beyond the scope of our work.

As we explain in the next paragraph, the structural representations from the previous layer, $\mathbf{h}_u^{(l-1)}(t)$, have integrated with the semantic representations. Consequently, the message-passing aggregation in Eq. 5 enables the propagation between both types of information, effectively facilitating semantic-structural reinforcement during encoding.

Cross-modal Mixer. Finally, we introduce a novel cross-modal mixer to automatically transfer and integrate information between the semantic and structural representations obtained at the l -th layer.

For node u at the l -th layer, the inputs of our cross-modal mixer are the most recent pre-mixed semantic representation $\tilde{\mathbf{e}}_u^{(l)}(t_k)$ and the corresponding pre-mixed structural representation $\tilde{\mathbf{h}}_u^{(l)}(t)$. This means that the remaining historical semantic representations, i.e., $\tilde{\mathbf{e}}_u^{(l)}(t_1), \dots, \tilde{\mathbf{e}}_u^{(l)}(t_{k-1})$, will be not involved in the mixture process. Such design is driven by: (i) efficiency consideration; (ii) temporal-awareness consideration that the latest semantic representation carries the

most contextually relevant information; and (iii) empirical consideration that mixing all semantic representations does not necessarily lead to better performance (See Sec. 4.5). Therefore, we concatenate $\tilde{\mathbf{e}}_u^{(l)}(t_k)$ with $\tilde{\mathbf{h}}_u^{(l)}(t)$, then pass through our cross-modal mixer, and finally split the fused representation to derive the post-mixed semantic and structural representations, respectively. These processes can be formulated as follows:

$$\mathbf{e}_u^{(l)}(t_k); \mathbf{h}_u^{(l)}(t) = \text{Mixer}^{(l)}(\tilde{\mathbf{e}}_u^{(l)}(t_k) \parallel \tilde{\mathbf{h}}_u^{(l)}(t)). \quad (9)$$

We implement $\text{Mixer}^{(l)}(\cdot)$ using a 2-layer MLP, and it can be alternatively conducted in other fusion components. By iteratively performing such a mixture operation, we can deeply unify both text semantics and graph structures, enabling effective representations for TTAG modeling.

3.3. Training

Output Layer. For node u at time t , its final representation is derived from three folds: (i) semantic outputs from the L -th semantic layer followed by the mean pooling, $\mathbf{z}_u^{\text{sem}}(t) = \text{Mean}(\tilde{\mathbf{e}}_u^{(L)}(t_1), \dots, \tilde{\mathbf{e}}_u^{(L)}(t_k))$; (ii) structural outputs from the L -th structural layer, $\mathbf{z}_u^{\text{str}}(t) = \tilde{\mathbf{h}}_u^{(L)}(t)$; and (iii) the unified outputs from our cross-modal mixer, $\mathbf{z}_u^{\text{mix}}(t) = \mathbf{e}_u^{(L)}(t_k) \parallel \mathbf{h}_u^{(L)}(t)$. The computations of our output layer for the final representation can be denoted as:

$$\mathbf{z}_u(t) = \text{MLP}_{\text{out}}(\mathbf{z}_u^{\text{sem}}(t) \parallel \mathbf{z}_u^{\text{str}}(t) \parallel \mathbf{z}_u^{\text{mix}}(t)), \quad (10)$$

where $\mathbf{z}_u(t) \in \mathbb{R}^d$ and $\text{MLP}_{\text{out}}(\cdot)$ is a 2-layer MLP that maps the dimension of the input vector to d .

Loss Function. We follow existing TGNNs (Zhang et al., 2024b) and adopt the temporal link prediction task as the training signal for TTAG modeling. Specifically, for each link (u, v, t) , we compute its occurrence probability $\hat{p}_{uv}(t)$ by feeding the concatenated representations of nodes u and v , i.e., $\mathbf{z}_u(t) \parallel \mathbf{z}_v(t)$, into a 2-layer MLP. The cross-entropy loss is then employed as our loss function:

$$\mathcal{L} = - \sum_{(u,v,t) \in \mathcal{G}} [\log \hat{p}_{uv}(t) + \log(1 - \hat{p}_{uv'}(t))]. \quad (11)$$

The v' is the randomly sampled negative destination node.

4. Experiments

4.1. Experimental Settings

Datasets. We implement experiments with five datasets, including four public datasets and one industrial dataset from real-world e-commerce systems. The four public datasets - Enron, GDELT, ICEWS1819, and Googlemap_CT - are recently collected and released by (Zhang et al., 2024a). Besides, the industrial dataset is constructed with three months of transaction data sampled from a private e-commercial

Table 1. MRR results (%) for temporal link prediction in transductive and inductive settings. The results for $\text{LLM}_{\text{zero/one}}$ represent the zero-shot or one-shot performance of the LLM DeepSeek-v2 (Liu et al., 2024). Results highlighted with a blue background indicate the performance after integrating CROSS into backbones and their corresponding improvements. The best results are highlighted in bold.

	Transductive setting					Inductive setting				
	Enron	GDELT	ICEWS1819	Googlemap_CT	Industrial	Enron	GDELT	ICEWS1819	Googlemap_CT	Industrial
JODIE	66.69 ± 2.0	48.81 ± 1.1	71.47 ± 4.0	56.72 ± 0.7	49.75 ± 1.2	53.41 ± 2.5	37.90 ± 2.4	57.75 ± 7.1	55.21 ± 1.0	30.38 ± 0.3
DyRep	58.85 ± 7.9	45.61 ± 2.8	63.13 ± 3.6	49.04 ± 2.2	36.49 ± 0.9	42.95 ± 8.3	42.23 ± 3.1	50.42 ± 2.8	47.44 ± 2.5	25.47 ± 1.8
TCL	71.16 ± 0.7	59.49 ± 0.5	87.58 ± 0.3	68.98 ± 0.4	50.87 ± 0.5	55.28 ± 1.5	47.13 ± 1.0	77.06 ± 0.2	66.26 ± 0.2	33.42 ± 0.5
CAWN	74.56 ± 0.6	57.00 ± 0.2	82.93 ± 0.1	65.34 ± 0.2	63.58 ± 0.8	61.58 ± 2.0	43.56 ± 0.6	70.65 ± 0.1	62.11 ± 0.2	53.42 ± 0.5
PINT	74.82 ± 2.8	52.71 ± 2.5	83.81 ± 0.9	72.94 ± 0.7	53.51 ± 0.6	56.38 ± 3.9	31.82 ± 4.1	63.16 ± 2.8	70.02 ± 0.6	39.72 ± 0.6
GraphMixer	62.68 ± 1.3	53.33 ± 0.4	80.69 ± 0.3	53.11 ± 0.2	50.50 ± 0.5	43.75 ± 1.5	41.18 ± 0.3	67.09 ± 0.5	51.36 ± 0.2	34.06 ± 0.7
FreeDyG	81.52 ± 1.8	68.27 ± 0.7	86.31 ± 0.6	78.82 ± 1.2	75.91 ± 0.7	70.38 ± 0.1	52.71 ± 0.3	74.16 ± 0.4	76.01 ± 2.8	76.48 ± 0.6
LLM_{zero}	24.18	7.99	33.68	30.30	11.27	17.73	10.08	32.26	38.21	2.62
LLM_{one}	46.27	28.91	50.82	48.79	30.29	48.14	28.91	44.69	43.83	20.28
TGAT	66.06 ± 0.1	56.73 ± .04	85.81 ± 0.2	63.13 ± 0.5	46.74 ± 3.9	47.80 ± 0.8	42.01 ± 0.5	74.10 ± 0.2	60.96 ± 0.2	30.04 ± 3.0
TGAT+	95.58 ± 0.7	81.63 ± 1.7	93.05 ± 1.6	99.91 ± 0.0	86.97 ± 2.8	81.52 ± 2.0	64.56 ± 1.8	82.25 ± 2.0	91.59 ± .03	62.22 ± 2.1
Avg. ↑ 26.59	↑ 29.52	↑ 24.90	↑ 7.24	↑ 36.78	↑ 40.23	↑ 33.72	↑ 22.55	↑ 8.15	↑ 30.63	↑ 32.18
TGN	73.05 ± 1.7	54.28 ± 1.6	84.79 ± 0.6	71.35 ± 0.5	54.46 ± 3.0	54.98 ± 2.3	37.48 ± 2.8	69.69 ± 0.8	67.88 ± 0.2	38.28 ± 4.1
TGN+	95.84 ± 0.4	77.95 ± 2.8	94.74 ± 5.7	99.92 ± 0.0	94.26 ± 0.8	82.38 ± 1.2	56.65 ± 3.8	84.01 ± 9.2	92.68 ± .08	83.23 ± 2.6
Avg. ↑ 25.45	↑ 22.79	↑ 23.67	↑ 9.95	↑ 28.57	↑ 39.80	↑ 27.40	↑ 19.17	↑ 14.32	↑ 24.80	↑ 44.02
DyGFormer	79.93 ± 0.1	61.35 ± 0.3	87.51 ± 0.3	54.82 ± 2.7	74.45 ± 0.7	66.86 ± 0.1	50.61 ± 0.2	78.14 ± 0.3	52.98 ± 2.5	54.20 ± 0.4
DyGFormer+	95.31 ± 2.8	81.28 ± 4.4	95.77 ± 0.3	99.82 ± 0.0	94.78 ± 1.4	86.01 ± 4.9	66.37 ± 4.4	87.80 ± 0.6	91.74 ± .09	82.30 ± 1.2
Avg. ↑ 22.03	↑ 15.38	↑ 19.93	↑ 8.26	↑ 44.99	↑ 20.33	↑ 19.15	↑ 15.76	↑ 9.66	↑ 38.76	↑ 28.10

trading network in XXX¹ Mobile Payment.² Details of the datasets are summarized in Sec. D.1 due to page limitations. All datasets are chronologically split by 60%, 20%, and 20% for training, validation, and testing, respectively.

Baselines. We select ten existing TGNNs as our baselines, including JODIE (Kumar et al., 2019), DyRep (Trivedi et al., 2019), TGAT (Xu et al., 2020), TGN (Rossi et al., 2020a), CAWN (Wang et al., 2021e), PINT (Souza et al., 2022), TCL (Wang et al., 2021a), GraphMixer (Cong et al., 2023), DyGFormer (Yu et al., 2023), and FreeDyG (Tian et al., 2024a). We also select powerful DeepSeek-v2 (Liu et al., 2024) and evaluate its zero-shot and one-shot performance as LLM baselines, denoted as $\text{LLM}_{\text{zero/one}}$. Detailed descriptions of all baselines are provided in Sec. D.2. Moreover, we choose three representative TGNN models, *i.e.*, TGAT, TGN, and DyGFormer, as the backbones of CROSS due to their superiority. For simplicity, we employ MiniLM (Wang et al., 2020) to embed all texts into feature space, and adopt DeepSeek-v2 as the LLM used in CROSS through a Language Model as a Service (LMaaS) compatible manner. We evaluate the learned representations using two downstream tasks, *i.e.*, temporal link prediction and node classification in an industrial application of financial risk management.

4.2. Temporal Link Prediction

We begin our experimental evaluation by comparing the temporal link prediction performance of our model with

¹The company name is anonymized for double-blind review. It will be disclosed in camera-ready if this paper can be accepted.

²The dataset is sampled solely for experimental purposes and does not imply any commercial affiliation. All personally identifiable information (PII) has been removed.

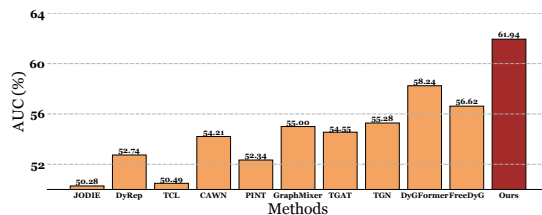


Figure 3. AUC results (%) for node classification of a real-world industrial application in financial risk management, which predicts whether nodes are involved in fraudulent activities on Industrial.

baselines. We conduct this under two settings: (i) **transductive** setting, which predicts links between nodes that have appeared during training; and (ii) **inductive** setting, where predictions are performed with unseen nodes. Implementation details can be found in Sec. D.3 of the Appendix.

The results are presented in Tab. 1. Clearly, we can observe that all three backbones exhibit significant performance improvements after integrating CROSS across all datasets in both transductive and inductive settings. Meanwhile, they achieve SOTA performance with a substantial margin over the best baseline. This observation proves the effectiveness of unifying text semantics and graph structures in TTAG modeling. Although LLM’s zero/one-shot performance is suboptimal, CROSS still performs well. This suggests that LLM may struggle to directly comprehend the dynamic graph structures within TTAGs, but it can effectively boost representation learning by providing temporal semantic information. Moreover, integrating CROSS tends to result in closer performance across models. We infer that this is due to the robustness of text semantics, which successfully reduces model reliance on simplistic structural information. Inspired by this, we detail a robustness study in Sec. 4.4.

Table 2. Ablation study for the raw texts and LLM-generated texts. **Semantic/Structural Encoding** refer to the encoding mechanisms that independently perform semantic/structural layers in Sec. 3.2; **imprv.** indicates the performance improvements of LLM-generated texts Text_{LLM} over the raw texts Text_{raw} . Our model can unlock the full potential of LLM-generated texts and achieve the best performance.

	Datasets	Methods	Semantic Encoding			Structural Encoding			Semantic-structural Co-encoding		
			Text_{raw}	Text_{LLM}	<i>imprv.</i>	Text_{raw}	Text_{LLM}	<i>imprv.</i>	Text_{raw}	Text_{LLM} (ours)	<i>imprv.</i>
Transductive	Enron	TGAT	49.73 ± 0.8	63.07 ± 0.5	↑ 13.34	66.06 ± 0.1	63.65 ± 1.7	↓ 2.41	70.27 ± 0.2	95.58 ± 0.7	↑ 25.31
		TGN	49.73 ± 0.8	63.07 ± 0.5	↑ 13.34	73.05 ± 1.7	72.36 ± 4.0	↓ 0.69	74.28 ± 0.9	95.84 ± 0.4	↑ 21.56
		DyGFormer	49.73 ± 0.8	63.07 ± 0.5	↑ 13.34	79.93 ± 0.1	80.46 ± 0.5	↑ 0.53	80.91 ± 0.1	95.31 ± 2.8	↑ 14.40
	ICEWS1819	TGAT	77.45 ± 0.5	85.04 ± 1.5	↑ 7.59	85.81 ± 0.2	86.12 ± 0.1	↑ 0.31	87.33 ± 1.0	93.05 ± 1.6	↑ 5.72
		TGN	77.45 ± 0.5	85.04 ± 1.5	↑ 7.59	84.79 ± 0.6	85.69 ± 0.4	↑ 0.90	85.96 ± 0.8	94.74 ± 5.7	↑ 8.78
		DyGFormer	77.45 ± 0.5	85.04 ± 1.5	↑ 7.59	87.51 ± 0.3	88.11 ± 0.5	↑ 0.60	86.72 ± 0.4	95.77 ± 0.3	↑ 9.05
Inductive	Enron	TGAT	31.94 ± 0.7	45.24 ± 1.1	↑ 13.30	47.80 ± 0.8	45.01 ± 1.3	↓ 2.79	53.26 ± 1.0	81.52 ± 2.0	↑ 28.26
		TGN	31.94 ± 0.7	45.24 ± 1.1	↑ 13.30	54.98 ± 2.3	53.93 ± 4.0	↓ 1.05	58.92 ± 1.4	82.38 ± 1.2	↑ 23.46
		DyGFormer	31.94 ± 0.7	45.24 ± 1.1	↑ 13.30	66.86 ± 0.1	67.64 ± 1.4	↑ 0.78	68.27 ± 0.1	86.01 ± 4.9	↑ 17.74
	ICEWS1819	TGAT	60.63 ± 0.8	71.45 ± 0.6	↑ 10.82	74.10 ± 0.2	74.12 ± 0.2	↑ 0.02	75.19 ± 0.2	82.25 ± 2.0	↑ 7.06
		TGN	60.63 ± 0.8	71.45 ± 0.6	↑ 10.82	69.69 ± 0.8	70.39 ± 1.2	↑ 0.70	70.01 ± 0.6	84.01 ± 9.2	↑ 13.99
		DyGFormer	60.63 ± 0.8	71.45 ± 0.6	↑ 10.82	78.14 ± 0.3	77.70 ± 0.8	↓ 0.44	79.79 ± 0.4	87.80 ± 0.6	↑ 8.01

4.3. Industrial Application

We conduct another downstream task using node classification in a real-world industrial application of financial risk management on Industrial, where we predict whether a node is involved in fraudulent activity. We employ DyGFormer as the backbone, and other details can be seen in Sec. D.3 of the Appendix. Our proposed method achieves the best performance as shown in Fig. 3, indicating that the learned representations of CROSS are also effective for the node classification task. This further validates CROSS’s applicability and practicality in real-world industrial scenarios.

4.4. Robustness Study

Robustness for noise. As stated in Sec. 1, the learned representations from existing TGNNs may rely solely on noisy structural information. To empirically validate this assumption, we strategically introduce noise into graph structures surrounding a target node by replacing its neighbors with randomly sampled nodes at perturbation rates of $p \in \{10\%, 20\%, 30\%, 40\%, 50\%\}$. To further investigate the impact of noise and assess the model ability to handle such conditions, we randomly select a subset of nodes and visualize the attention weights of their perturbed neighbors during encoding using box plots under $p = 50\%$.

We report the results in Figs. 4 and 5. The boosted models consistently perform best and exhibit remarkable robustness even under high perturbation rates. This may be owing to CROSS’s ability to effectively harness the valuable temporal semantic information, which aids in mitigating the adverse impact of structural noise attacks. Furthermore, the results of attention weights reveal that the boosted models can effectively down-weight the noisy neighbors during encoding. This may be the key reason why CROSS could achieve superior performance and exceptional robustness. These results also strongly support the underlying motivation for unifying text semantics and graph structures in TTAG modeling.

Robustness for encoding layers. Next, we study the model

robustness to the number of encoding layers. Specifically, we conduct a series of experiments with varying numbers of encoding layers $L = \{1, 2, 3, 4, 5\}$. A larger number of encoding layers facilitates a deeper integration of the cross-modal information. We employ TGAT and TGN as the backbones in this group of experiments. Notably, unlike previous experiments, we set the neighbor sampling size in each layer to 5 due to computational constraints. All other hyper-parameters remain set to their default values detailed in Sec D.3 of the Appendix.

The results are depicted in Fig. 6. The boosted models also demonstrate outstanding robustness to the encoding layers, where the performance improvements over their respective backbones become more pronounced as the number of layers increases. Such robustness likely stems from the invaluable semantic information and the sufficient fusion between semantics and structures, whereas single high-order graph structures tend to introduce much irrelevant or even spurious information. We also find that the boosted models always achieve their peak performance with a larger L . This can be attributed to the deeper information exchange of our cross-modal mixer, which fully amplifies the mutual reinforcement between semantics and structures.

4.5. Ablation Study

We conduct three sets of experiments in our ablation study.

Ablation for model components. We start the ablation study by evaluating the contributions of the key components of our model. Detailed information for each variant is provided in Sec. H of the Appendix. The results are detailed in Fig. 7. We can see that incorporating all components results in the best performance, while the removal of any single component leads to a performance drop. This highlights the effectiveness of each component in CROSS. Notably, mixing all semantic representations does not improve model performance. This may be attributed to the unexpected inclusion of overly outdated semantic information when

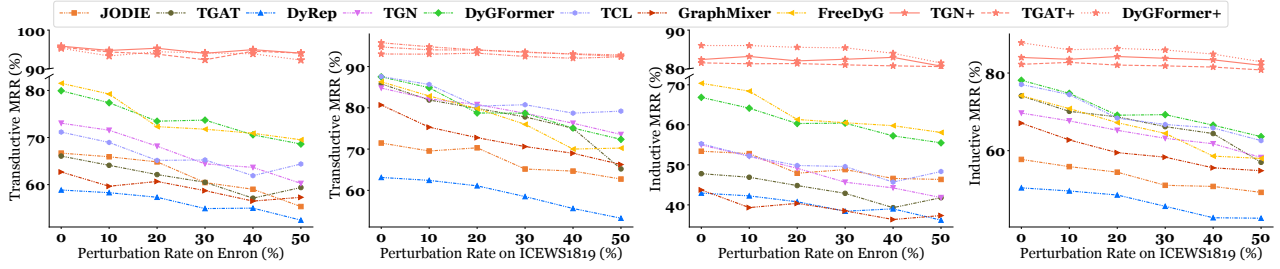


Figure 4. Robustness study for noise on Enron and ICEWS1819 with different perturbation rates.

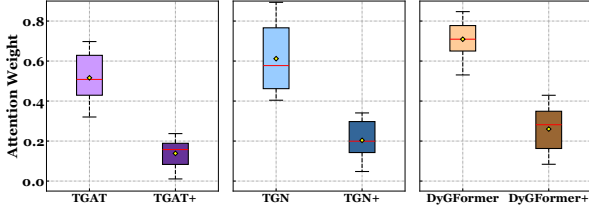


Figure 5. Attention weights from randomly selected nodes to their perturbed neighbors on GDELT with the perturbation rate of 50%.

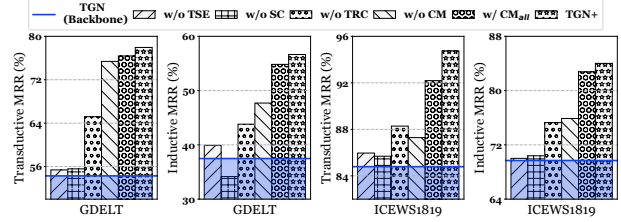


Figure 7. Ablation study for model components in boosted TGN model. The results for TGN backbone are included for reference.

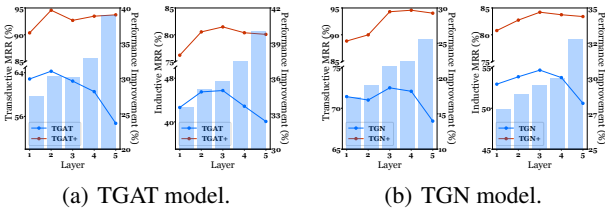


Figure 6. Robustness study for encoding layers on Enron.

passing through our cross-modal mixer, thus hindering the quality of the final representations.

Ablation for raw texts and LLM-generated texts. We then conduct an ablation study to compare the **raw texts** (*i.e.*, the original text attributes in TTAGs) with the **LLM-generated texts** (*i.e.*, neighborhood summaries produced by the LLM) using various encoding mechanisms. We present the results in Tab. 2 and other details can be seen in Sec. H. Firstly, our model outperforms all other variants, reaffirming its effectiveness. Besides, the results using semantic encoding prove the validity and expressiveness of the pure LLM-generated texts. Interestingly, the performance of LLM-generated texts yields only marginal improvements or even slight degradation when performing structural encoding. We infer that this occurs because the structural encoding introduces excessively irrelevant information from high-order relations, whereas the other two encodings directly capitalize on the node’s own LLM-generated texts, thus integrating more focused and relevant information. This demonstrates the necessity of an appropriate encoding mechanism and further highlights the superiority of our introduced Co-encoder.

Ablation for different LLMs. We extend our ablation study with various LLMs, including Llama3-8b (AI@Meta, 2024), Vicuna-7b (Chiang et al., 2023), and Mistral-7b (Jiang et al.,

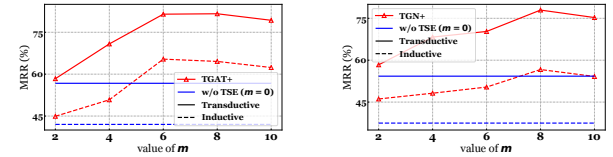


Figure 8. Parameter study with different maximum reasoning count m on GDELT. The results for w/o TSE are shown for reference.

2023). Details and results are put in Sec. H and Fig. 16, respectively. CROSS consistently performs best, reaffirming the effectiveness and robustness of our proposed framework.

4.6. Parameter Study

To balance granularity and efficiency, we set a maximum reasoning count (m in Eq. 1) to constrain the number of LLM reasoning steps. Now we study how this hyper-parameter impacts performance. We plot the results with varying m in Fig. 8. Reasoning too infrequently (small m) may make the LLM cannot effectively comprehend the semantic dynamics around nodes and thus result in degraded performance, while reasoning too frequently (large m) may cause the LLM to fail to capture long-term semantic shifts. It is also worth noting that different models exhibit varying sensitivities, and $m = 8$ seems to be a generally sweet choice.

5. Conclusion and Future Work

In this paper, we focus on an unexplored problem of TTAG modeling. To address this, we propose CROSS, which extends existing TGNs to effectively unify text semantics and graph structures for TTAG modeling with the help of LLMs. By introducing the LLM-based Temporal Semantics

Extractor, we can dynamically extract the text semantics within nodes' neighborhoods. The Semantic-structural Co-encoder then integrates semantic and structural information, enabling bidirectional reinforcement between both modalities. As for future work, we will consider more complex designs of our cross-modal mixer for achieving better representation fusion, such as using the time decay mechanism.

Impact Statement

This paper presents work whose goal is to advance the field of Machine Learning. There are many potential societal consequences of our work, none which we feel must be specifically highlighted here.

References

- AI@Meta. Llama 3 model card, 2024. Available online.
- Alvarez-Rodriguez, U., Battiston, F., de Arruda, G. F., Moreno, Y., Perc, M., and Latora, V. Evolutionary dynamics of higher-order interactions in social networks. *Nature Human Behaviour*, 5(5):586–595, 2021.
- Chang, X., Liu, X., Wen, J., Li, S., Fang, Y., Song, L., and Qi, Y. Continuous-time dynamic graph learning via neural interaction processes. In *Proceedings of the 29th ACM International Conference on Information & Knowledge Management*, pp. 145–154, 2020.
- Chen, Y., Zeng, A., Yu, Q., Zhang, K., Yuanpeng, C., Wu, K., Huzhang, G., Yu, H., and Zhou, Z. Recurrent temporal revision graph networks. *Advances in Neural Information Processing Systems*, 36, 2024a.
- Chen, Z., Mao, H., Li, H., Jin, W., Wen, H., Wei, X., Wang, S., Yin, D., Fan, W., Liu, H., et al. Exploring the potential of large language models (llms) in learning on graphs. *ACM SIGKDD Explorations Newsletter*, 25(2): 42–61, 2024b.
- Chiang, W.-L., Li, Z., Lin, Z., Sheng, Y., Wu, Z., Zhang, H., Zheng, L., Zhuang, S., Zhuang, Y., Gonzalez, J. E., et al. Vicuna: An open-source chatbot impressing gpt-4 with 90%* chatgpt quality. See <https://vicuna.lmsys.org> (accessed 14 April 2023), 2(3):6, 2023.
- Cong, W., Zhang, S., Kang, J., Yuan, B., Wu, H., Zhou, X., Tong, H., and Mahdavi, M. Do we really need complicated model architectures for temporal networks? *arXiv preprint arXiv:2302.11636*, 2023.
- Duan, Y., Liu, J., Chen, S., Chen, L., and Wu, J. G-prompt: Graphon-based prompt tuning for graph classification. *Information Processing & Management*, 61(3):103639, 2024.
- Fan, Z., Liu, Z., Zhang, J., Xiong, Y., Zheng, L., and Yu, P. S. Continuous-time sequential recommendation with temporal graph collaborative transformer. In *Proceedings of the 30th ACM international conference on information & knowledge management*, pp. 433–442, 2021.
- Fang, Y., Fan, D., Zha, D., and Tan, Q. Gaugllm: Improving graph contrastive learning for text-attributed graphs with large language models. In *Proceedings of the 30th ACM SIGKDD Conference on Knowledge Discovery and Data Mining*, pp. 747–758, 2024.
- Gao, J. and Ribeiro, B. On the equivalence between temporal and static equivariant graph representations. In *International Conference on Machine Learning*, pp. 7052–7076. PMLR, 2022.
- Goyal, P., Chhetri, S. R., and Canedo, A. dyngraph2vec: Capturing network dynamics using dynamic graph representation learning. *Knowledge-Based Systems*, 187: 104816, 2020.
- He, X., Bresson, X., Laurent, T., Perold, A., LeCun, Y., and Hooi, B. Harnessing explanations: Llm-to-llm interpreter for enhanced text-attributed graph representation learning. *arXiv preprint arXiv:2305.19523*, 2023.
- He, X., Tian, Y., Sun, Y., Chawla, N. V., Laurent, T., LeCun, Y., Bresson, X., and Hooi, B. G-retriever: Retrieval-augmented generation for textual graph understanding and question answering. *arXiv preprint arXiv:2402.07630*, 2024.
- Huang, S., Poursafaei, F., Danovitch, J., Fey, M., Hu, W., Rossi, E., Leskovec, J., Bronstein, M., Rabusseau, G., and Rabbany, R. Temporal graph benchmark for machine learning on temporal graphs. *Advances in Neural Information Processing Systems*, 36, 2024.
- Jiang, A. Q., Sablayrolles, A., Mensch, A., Bamford, C., Chaplot, D. S., Casas, D. d. l., Bressand, F., Lengyel, G., Lample, G., Saulnier, L., et al. Mistral 7b. *arXiv preprint arXiv:2310.06825*, 2023.
- Jin, B., Zhang, W., Zhang, Y., Meng, Y., Zhang, X., Zhu, Q., and Han, J. Patton: Language model pretraining on text-rich networks. *arXiv preprint arXiv:2305.12268*, 2023a.
- Jin, B., Zhang, Y., Meng, Y., and Han, J. Edgeformers: Graph-empowered transformers for representation learning on textual-edge networks. *arXiv preprint arXiv:2302.11050*, 2023b.
- Jin, B., Zhang, Y., Zhu, Q., and Han, J. Heterformer: Transformer-based deep node representation learning on heterogeneous text-rich networks. In *Proceedings of the 29th ACM SIGKDD Conference on Knowledge Discovery and Data Mining*, pp. 1020–1031, 2023c.
- Kazemi, S. M., Goel, R., Eghbali, S., Ramanan, J., Sahota, J., Thakur, S., Wu, S., Smyth, C., Poupart, P., and Brubaker, M. Time2vec: Learning a vector representation of time. *arXiv preprint arXiv:1907.05321*, 2019.
- Kumar, S., Zhang, X., and Leskovec, J. Predicting dynamic embedding trajectory in temporal interaction networks.

- In *Proceedings of the 25th ACM SIGKDD international conference on knowledge discovery & data mining*, pp. 1269–1278, 2019.
- Li, X., Lian, D., Lu, Z., Bai, J., Chen, Z., and Wang, X. Graphadapter: Tuning vision-language models with dual knowledge graph. *Advances in Neural Information Processing Systems*, 36, 2024.
- Liu, A., Feng, B., Wang, B., Wang, B., Liu, B., Zhao, C., Deng, C., Ruan, C., Dai, D., Guo, D., et al. Deepseek-v2: A strong, economical, and efficient mixture-of-experts language model. *arXiv preprint arXiv:2405.04434*, 2024.
- Luo, Y. and Li, P. Neighborhood-aware scalable temporal network representation learning. In *Learning on Graphs Conference*, pp. 1–1. PMLR, 2022.
- Pareja, A., Domeniconi, G., Chen, J., Ma, T., Suzumura, T., Kanezashi, H., Kaler, T., Schardl, T., and Leiserson, C. Evolvegn: Evolving graph convolutional networks for dynamic graphs. In *Proceedings of the AAAI conference on artificial intelligence*, volume 34, pp. 5363–5370, 2020.
- Ren, X., Wei, W., Xia, L., Su, L., Cheng, S., Wang, J., Yin, D., and Huang, C. Representation learning with large language models for recommendation. In *Proceedings of the ACM on Web Conference 2024*, pp. 3464–3475, 2024.
- Rossi, E., Chamberlain, B., Frasca, F., Eynard, D., Monti, F., and Bronstein, M. Temporal graph networks for deep learning on dynamic graphs. *arXiv preprint arXiv:2006.10637*, 2020a.
- Rossi, R. A., Zhou, R., and Ahmed, N. K. Deep inductive graph representation learning. *IEEE Transactions on Knowledge and Data Engineering*, 32(3):438–452, 2020b. doi: 10.1109/TKDE.2018.2878247.
- Souza, A., Mesquita, D., Kaski, S., and Garg, V. Provably expressive temporal graph networks. *Advances in Neural Information Processing Systems*, 35:32257–32269, 2022.
- Tan, Y., Zhou, Z., Lv, H., Liu, W., and Yang, C. Walklm: A uniform language model fine-tuning framework for attributed graph embedding. *Advances in Neural Information Processing Systems*, 36, 2024.
- Tang, J., Yang, Y., Wei, W., Shi, L., Su, L., Cheng, S., Yin, D., and Huang, C. Graphgpt: Graph instruction tuning for large language models. In *Proceedings of the 47th International ACM SIGIR Conference on Research and Development in Information Retrieval*, pp. 491–500, 2024.
- Tian, Y., Qi, Y., and Guo, F. Freedyg: Frequency enhanced continuous-time dynamic graph model for link prediction. In *The Twelfth International Conference on Learning Representations*, 2024a. URL <https://openreview.net/forum?id=82Mc5ilInM>.
- Tian, Y., Song, H., Wang, Z., Wang, H., Hu, Z., Wang, F., Chawla, N. V., and Xu, P. Graph neural prompting with large language models. In *Proceedings of the AAAI Conference on Artificial Intelligence*, volume 38, pp. 19080–19088, 2024b.
- Trivedi, R., Farajtabar, M., Biswal, P., and Zha, H. Dyrep: Learning representations over dynamic graphs. In *International conference on learning representations*, 2019.
- Vaswani, A., Shazeer, N., Parmar, N., Uszkoreit, J., Jones, L., Gomez, A. N., Kaiser, Ł., and Polosukhin, I. Attention is all you need. *Advances in neural information processing systems*, 30, 2017.
- Wang, L., Chang, X., Li, S., Chu, Y., Li, H., Zhang, W., He, X., Song, L., Zhou, J., and Yang, H. Tcl: Transformer-based dynamic graph modelling via contrastive learning. *arXiv preprint arXiv:2105.07944*, 2021a.
- Wang, W., Wei, F., Dong, L., Bao, H., Yang, N., and Zhou, M. Minilm: Deep self-attention distillation for task-agnostic compression of pre-trained transformers. *Advances in Neural Information Processing Systems*, 33: 5776–5788, 2020.
- Wang, X., Lyu, D., Li, M., Xia, Y., Yang, Q., Wang, X., Wang, X., Cui, P., Yang, Y., Sun, B., et al. Apan: Asynchronous propagation attention network for real-time temporal graph embedding. In *Proceedings of the 2021 international conference on management of data*, pp. 2628–2638, 2021b.
- Wang, Y., Cai, Y., Liang, Y., Ding, H., Wang, C., Bhatia, S., and Hooi, B. Adaptive data augmentation on temporal graphs. *Advances in Neural Information Processing Systems*, 34:1440–1452, 2021c.
- Wang, Y., Cai, Y., Liang, Y., Ding, H., Wang, C., and Hooi, B. Time-aware neighbor sampling for temporal graph networks. *arXiv preprint arXiv:2112.09845*, 2021d.
- Wang, Y., Chang, Y.-Y., Liu, Y., Leskovec, J., and Li, P. Inductive representation learning in temporal networks via causal anonymous walks. *arXiv preprint arXiv:2101.05974*, 2021e.
- Wen, Z. and Fang, Y. Trend: Temporal event and node dynamics for graph representation learning. In *Proceedings of the ACM Web Conference 2022*, pp. 1159–1169, 2022.
- Xiang, S., Zhu, M., Cheng, D., Li, E., Zhao, R., Ouyang, Y., Chen, L., and Zheng, Y. Semi-supervised credit card fraud detection via attribute-driven graph representation.

- In *Proceedings of the AAAI Conference on Artificial Intelligence*, volume 37, pp. 14557–14565, 2023.
- Xu, D., Ruan, C., Korpeoglu, E., Kumar, S., and Achan, K. Inductive representation learning on temporal graphs. *arXiv preprint arXiv:2002.07962*, 2020.
- Yang, J., Liu, Z., Xiao, S., Li, C., Lian, D., Agrawal, S., Singh, A., Sun, G., and Xie, X. Graphformers: Gnn-nested transformers for representation learning on textual graph. *Advances in Neural Information Processing Systems*, 34:28798–28810, 2021.
- Yasunaga, M., Leskovec, J., and Liang, P. Linkbert: Pre-training language models with document links. *arXiv preprint arXiv:2203.15827*, 2022.
- Yu, L., Sun, L., Du, B., and Lv, W. Towards better dynamic graph learning: New architecture and unified library. *arXiv preprint arXiv:2303.13047*, 2023.
- Zhang, J., Chen, J., Yang, M., Feng, A., Liang, S., Shao, J., and Ying, R. Dtg: A comprehensive benchmark for dynamic text-attributed graphs. *Advances in Neural Information Processing Systems*, 2024a.
- Zhang, S., Chen, X., Xiong, Y., Wu, X., Zhang, Y., Fu, Y., Zhao, Y., and Zhang, J. Towards adaptive neighborhood for advancing temporal interaction graph modeling. In *Proceedings of the 30th ACM SIGKDD Conference on Knowledge Discovery and Data Mining*, pp. 4290–4301, 2024b.
- Zhang, X., Bosselut, A., Yasunaga, M., Ren, H., Liang, P., Manning, C. D., and Leskovec, J. Greaselm: Graph reasoning enhanced language models for question answering. *arXiv preprint arXiv:2201.08860*, 2022.
- Zhang, Y., Xiong, Y., Liao, Y., Sun, Y., Jin, Y., Zheng, X., and Zhu, Y. Tiger: Temporal interaction graph embedding with restarts. In *ACM Web Conference*, 2023.
- Zhang, Z., Wang, X., Zhang, Z., Li, H., Qin, Y., and Zhu, W. Llm4dyg: Can large language models solve spatial-temporal problems on dynamic graphs? In *Conference on Knowledge Discovery and Data Mining (ACM SIGKDD)*, 2024c.
- Zhao, J., Qu, M., Li, C., Yan, H., Liu, Q., Li, R., Xie, X., and Tang, J. Learning on large-scale text-attributed graphs via variational inference. *arXiv preprint arXiv:2210.14709*, 2022.
- Zhou, H., Zheng, D., Nisa, I., Ioannidis, V., Song, X., and Karypis, G. Tgl: A general framework for temporal gnn training on billion-scale graphs. *arXiv preprint arXiv:2203.14883*, 2022.
- Zhu, Y., Wang, Y., Shi, H., and Tang, S. Efficient tuning and inference for large language models on textual graphs. *arXiv preprint arXiv:2401.15569*, 2024.
- Zou, W., Hu, X., Pan, Z., Li, C., Cai, Y., and Liu, M. Exploring the relationship between social presence and learners’ prestige in mooc discussion forums using automated content analysis and social network analysis. *Computers in Human Behavior*, 115:106582, 2021.

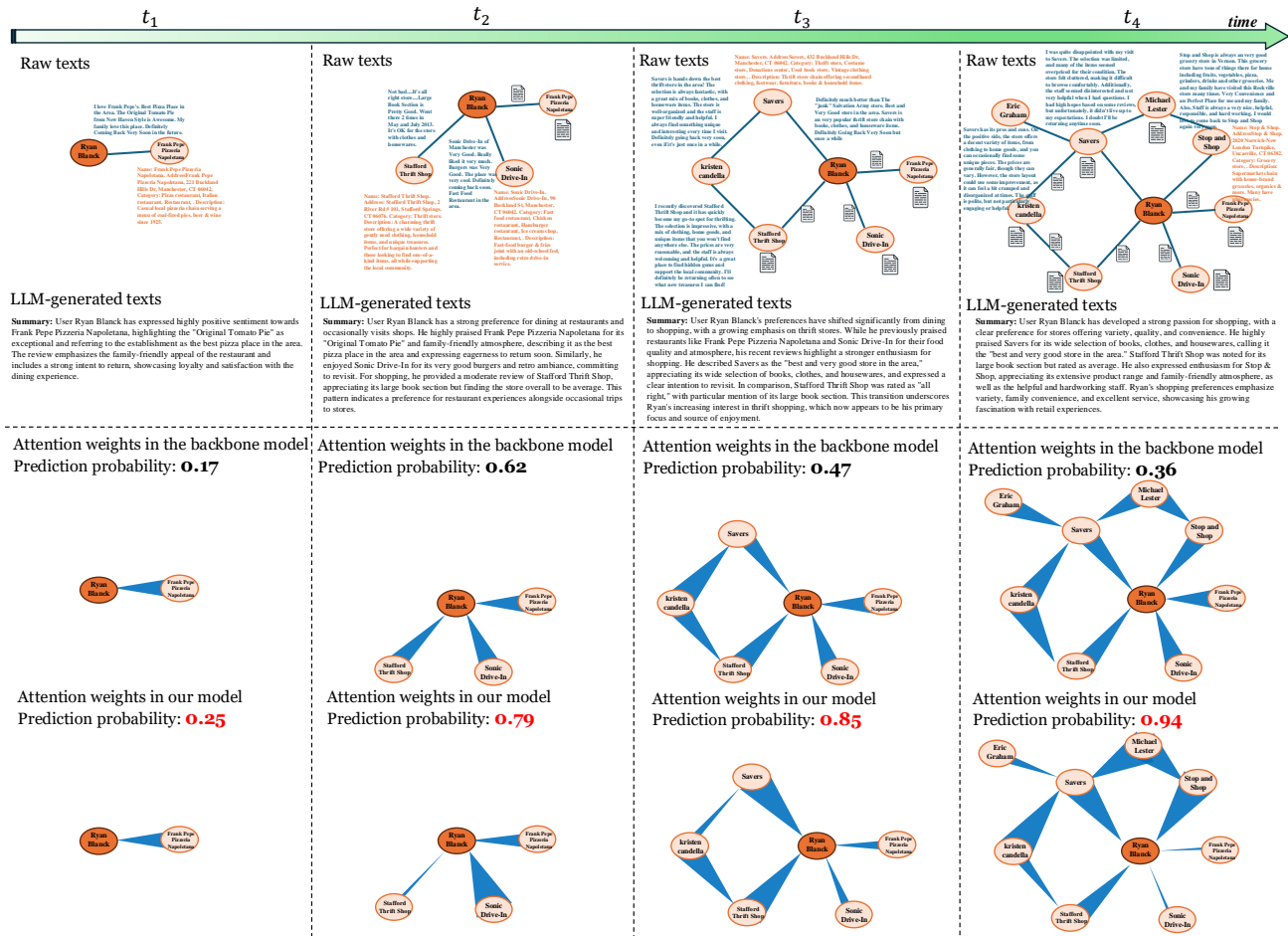


Figure 9. Case study on Golemap_CT with TGAT model, where we visualize the raw texts in TTAGs, the LLM-generated texts produced by the Temporal Semantics Extractor, the attention weights assigned among neighborhoods by the backbone and our model during encoding, and the corresponding prediction probability. Thicker edges denote higher attention weights. **CROSS exhibits exceptional prediction performance and robustness** by successfully unifying semantics and structures, which enables the model to adaptively adjust the attention weights of neighbors, thereby generating more optimal representations and achieving improved prediction performance.

A. Case Study

In this section, we conduct a case study to investigate the essence of the effectiveness of CROSS. As illustrated in Fig. 9, we select a representative example node from the Golemap_CT dataset and visualize the raw texts in TTAGs, the LLM-generated texts produced by our Temporal Semantics Extractor, the attention weights assigned among neighborhoods by the backbone and our model during encoding, and the corresponding prediction probability. The value of prediction probability refers to the predicted probability for the corresponding positive edges as defined in Eq. 11, where higher values indicate better performance. For clarity, our visualization is restricted to the 2-hop neighborhoods of the target node.

We observe that CROSS demonstrates a remarkable ability to capture semantic dynamics, which allows the model to adaptively adjust attention weights among neighborhoods during encoding, thereby achieving improved prediction performance. For instance, CROSS effectively detects the semantic shift in preferences for the target node “Ryan Blanck” across temporal dimensions, which is from “restaurant” to “shopping” ($t_2 \rightarrow t_3$). Subsequently, it automatically reduces the attention weights assigned to restaurant nodes (e.g., “Frank Pepe Pizzeria Napoletana”) while increasing the weight for store-related neighbors (e.g., “Stafford Thrift Shop”). This shows that the dynamic semantic information enables the model to prioritize the most relevant neighbors at different timestamps, thereby generating optimal representations and improving the overall prediction performance. We also find that the backbone model exhibits inconsistent performance across different timestamps while our model showcases a steady and continuous improvement in performance. This can be attributed to the inherent robustness of semantic information, which provides greater stability compared to simplistic structural information.

B. Theoretical Analysis

In this section, we conduct a theoretical analysis to illustrate that the text semantics from LLM-generated texts can provide valuable information for the graph structures when unifying both of them. This holds true under two key conditions:

- *Integrity*: The text semantics derived from LLM-generated texts are deeply rooted in the LLM’s extensive parameterized knowledge, enabling them to accurately reflect the graph structures among neighborhoods for the target node.
- *Complementarity*: The text semantics from LLM-generated texts complement the graph structures among neighborhoods, providing additional perspectives that aid in distinguishing subtle relationships.

Theorem 1. *Consider the conditions as follows:*

1) *Integrity*: Z_T serves as a reliable proxy for Z_G , thus we have

$$H(Z_G|Z_T) = \epsilon, \quad \epsilon > 0. \quad (12)$$

2) *Complementarity*: Z_T encapsulates orthogonal information that is not captured by Z_G , and that is

$$H(y|Z_G, Z_T) = H(y|Z_G) - \epsilon', \quad \epsilon' > \epsilon. \quad (13)$$

Under these conditions, it follows that:

$$H(y|Z_G, Z_T) < H(y|Z_G), \quad (14)$$

where Z_G denotes the information derived from graph structures, Z_T represents the information captured from text semantics, y is the target for prediction, and $H(\cdot|\cdot)$ depicts the condition entropy.

Proof. We aim to prove that the conditional entropy of y unifying both graph structures Z_G and text semantics Z_T , i.e., $H(y|Z_G, Z_T)$, is strictly less than the conditional entropy of y solely based on Z_G , i.e., $H(y|Z_G)$.

We begin with:

$$H(y|Z_G, Z_T). \quad (15)$$

Next, we decompose this using the properties of entropy into two phases:

$$H(y|Z_G, Z_T) = H(y|Z_G, Z_M, Z_T) + I(y; Z_M|Z_G, Z_T), \quad (16)$$

where Z_M denotes the information arising from the mixed representations of text semantics and graph structures.

We then apply the following upper bound on conditional mutual information as follows:

$$\begin{aligned} I(y; Z_M|Z_G, Z_T) &= H(Z_M|Z_G, Z_T) - H(Z_M|y, Z_G, Z_T) \\ &\leq H(Z_M|Z_G, Z_T). \end{aligned} \quad (17)$$

Here, the first equality follows from the definition of mutual information, and the inequality holds due to the nonnegativity of conditional entropy.

By substituting Eq. 17 into Eq. 16, we obtain:

$$H(y|Z_G, Z_T) \leq H(y|Z_G, Z_M, Z_T) + H(Z_M|Z_G, Z_T). \quad (18)$$

Since conditional entropy increases when conditioning on fewer variables, it follows that:

$$H(y|Z_G, Z_M, Z_T) + H(Z_M|Z_G, Z_T) \leq H(y|Z_G, Z_T) + H(Z_G|Z_T). \quad (19)$$

By applying the ‘‘Integrity’’ and ‘‘Complementarity’’ conditions, we arrive at:

$$H(y|Z_G, Z_M) + H(Z_M|Z_T) \leq H(y|Z_G) - \epsilon' + \epsilon. \quad (20)$$

Finally, since $\epsilon' > \epsilon$, we conclude:

$$H(y|Z_G) - \epsilon' + \epsilon < H(y|Z_G). \quad (21)$$

Consequently, we have proven that:

$$H(y|Z_G, Z_T) < H(y|Z_G). \quad (22)$$

This completes the proof. \square

Algorithm 1: Training CROSS (one epoch).

Input: A node set \mathcal{V} ; A TTAG $\mathcal{G} = \{(u, v, t)\}$ with node text attributes \mathcal{D} and edge text attributes \mathcal{R} ; The maximum reasoning count m ; The number of encoding layer L .

- 1 Initialize all model parameters and prepare the LLM;
// Temporal Semantics Extractor
- 2 **foreach** $u \in \mathcal{V}$ **do**
- 3 Derive reasoning timestamps $\hat{\mathcal{T}}_u$ with m by Eq. 1;
- 4 Summarize u 's textualized neighborhood at $\hat{t} \in \hat{\mathcal{T}}_u$ with LLM by Eq. 2;
- 5 **end**
// Semantic-structural Co-encoder
- 6 **foreach** $batch (u, v, t) \subseteq \mathcal{G}$ **do**
- 7 **foreach** $l = 1, 2, \dots, L$ **do**
- 8 Retrieve text semantics from generated summaries and graph structures from neighborhoods for nodes u/v ;
- 9 Compute pre-mixed semantic representations $\tilde{\mathbf{e}}_{u/v}^{(l)}(t_k)$ with semantic layer by Eqs. 3-4;
- 10 Compute pre-mixed structural representations $\tilde{\mathbf{h}}_{u/v}^{(l)}(t)$ with structural layer by Eqs. 5-8;
- 11 Mix and propagate cross-modal representations by Eq. 9;
- 12 **end**
- 13 Derive the final representations $\mathbf{z}_{u/v}(t)$ by Eq. 10;
- 14 Compute loss \mathcal{L} by Eq. 11 and backward;
- 15 **end**

C. Notations and Algorithms

We provide the important notations used in this paper and their corresponding descriptions as shown in Tab. 3. Additionally, for clarity, we present the pseudo-codes of CROSS in Algorithm 1.

Table 3. Important notations and descriptions.

Notations	Descriptions
d_u	Raw text attribute of node u
$r_{u,v,t}$	Raw text attribute of edge (u, v, t)
$\hat{d}_u(\hat{t})$	LLM-generated text summary for u 's neighborhood at reasoning time \hat{t}
$\tilde{\mathbf{e}}_u^{(l)}(t)$	Pre-mixed semantic representation for node u at time t in the l -th layer
$\mathbf{e}_u^{(l)}(t)$	Post-mixed semantic representation for node u at time t in the l -th layer
$\tilde{\mathbf{h}}_u^{(l)}(t)$	Pre-mixed structural representation for node u at time t in the l -th layer
$\mathbf{h}_u^{(l)}(t)$	Post-mixed structural representation for node u at time t in the l -th layer
$\mathbf{z}_u(t)$	Final representation for node u at time t

D. Details of Experimental Setting

D.1. Datasets

In this paper, we select four public datasets (Zhang et al., 2024a) from different domains and one real-world industrial dataset. We present their detailed descriptions below, and their statistics are summarized in Tab. 4.

- **GDELT**³ originates from a collection of email exchanges among employees of the ENRON energy corporation spanning three years (1999–2002). In this dataset, nodes represent employees, and edges correspond to emails exchanged between them. Each node has text attributes that are derived from the employee's department and role if

³<https://www.cs.cmu.edu/~enron/>

such information is available. Each edge attaches text attributes consisting of the raw content of the emails. Edges are sequentially ordered based on the e-mail sending timestamps.

- **Enron**⁴ originates from the Global Database of Events, Language, and Tone, a project aimed at cataloging political behaviors across nations worldwide. In this dataset, nodes represent political entities, such as “Egypt” or “Kim Jong Un”. The textual attributes of nodes are directly taken from the names of these entities. Edges capture the relationships between entities (e.g., “Make Empathetic Comment” or “Provide Aid”), with the textual attributes of edges being derived from the descriptions of these relationships. Edges are sequentially ordered based on the event-occurring timestamps.
- **ICEWS1819**⁵ is sourced from the Integrated Crisis Early Warning System project, which serves as a larger temporal knowledge graph for tracking political events compared to Enron. This dataset is built using events occurring between January 1, 2018, and December 31, 2019. The textual attributes of nodes include the name, sector, and nationality of each political entity, while the textual attributes of edges represent descriptions of the political relationships. All edges are sequentially ordered based on the event-occurring timestamps.
- **Googlemap_CT**⁶ is sourced from the Google Local Data project, which compiles review data from Google Maps along with user and business information in the United States up to September 2021. This dataset specifically focuses on business entities located in Connecticut. Nodes represent users and businesses, while edges correspond to user reviews of businesses. Textual attributes are assigned exclusively to business nodes, encompassing the business name, address, category, and self-introduction. All edges are sequentially ordered based on the review timestamps.
- **Industrial** is sourced from real-world e-commercial transaction records sampled from a mobile payment company, spanning March to June 2024. Nodes in this dataset represent users or merchants while edges denote their transaction records. Each node is enriched with text attributes, such as the user/merchant name and affiliation. Text attributes of each edge include textual details such as price, transaction type, and user review. Besides, all edges are sequentially ordered based on the transaction timestamps, and each node is assigned a **label** indicating whether it is fraudulent.

Table 4. Detailed statistics of datasets.

Datasets	# Nodes	# Links	# Times	Duration	Domains	Time Granularity
Enron	42,711	797,907	1,006	3 years	E-mail	one day
GDELT	6,786	1,339,245	2,591	2 years	knowledge graph	15 minutes
ICEWS1819	31,769	1,100,071	730	2 years	knowledge graph	24 hours
Googlemap_CT	111,168	1,380,623	55,521	–	Recommendation	Unix Time
Industrial	1,112,094	3,196,008	90	3 months	E-commerce	one day

D.2. Baselines

We evaluate the performance and discuss the capabilities of ten existing TGNNs. The details of these methods are as follows:

- **JODIE** (Kumar et al., 2019) is designed to manage temporal graphs in bipartite user-item settings. It employs two Recurrent Neural Networks (RNNs), one for updating the user states and another for the item states. To prevent the issue of outdated node representations, a projection layer is added to track the evolution of the embeddings over time.
- **DyRep** (Trivedi et al., 2019) incorporates neighborhood information by utilizing a temporal attention-based aggregation mechanism. This approach helps capture the evolving structural features of nodes’ local environments in the temporal graph, allowing for more accurate dynamic representations.
- **TGAT** (Xu et al., 2020) leverages a temporal attention model to aggregate data from temporal-topological neighbors, facilitating the creation of temporal node embeddings. It also introduces a trainable time encoding function that ensures each temporal step is distinctly represented, a concept widely adopted in later TGN architectures.

⁴<https://www.gdeltproject.org/>

⁵<https://dataverse.harvard.edu/dataverse/icews>

⁶https://datarepo.eng.ucsd.edu/mcauley_group/gdrive/googleglocal/

- **TGN** (Rossi et al., 2020a) builds upon earlier methodologies by introducing a memory system that stores a state vector for each node. This memory is refreshed whenever a node participates in an interaction. The model also features modules for processing messages, updating memory states, and embedding temporal features, which collectively enable the generation of dynamic node representations.
- **CAWN** (Wang et al., 2021e) creates node embeddings using temporal walks. It generates multiple anonymous random walks starting from a target node and encodes them using a Recurrent Neural Network. These encoded walks are then combined to form the final temporal representation, which is particularly effective for predicting temporal links.
- **TCL** (Wang et al., 2021a) uses a breadth-first search to form temporal dependency sub-graphs, extracting sequences of interactions for analysis. A Transformer encoder is applied to integrate temporal and structural information, enabling central node representation learning. Additionally, TCL incorporates a cross-attention mechanism within the Transformer to capture interdependencies between interacting node pairs.
- **PINT** (Souza et al., 2022) applies injective message passing with a temporal focus and incorporates relative positional encoding to improve the model’s capability in capturing dynamic patterns within neighborhoods.
- **GraphMixer** (Cong et al., 2023) employs a link encoder inspired by the MLP-Mixer framework to create temporal embeddings for nodes. Its design includes a fixed time encoding scheme, which demonstrates superior performance compared to traditional learnable approaches. The model also utilizes a node encoder with mean-pooling to aggregate link-based information.
- **DyGFormer** (Yu et al., 2023) relies on information from 1-hop neighbors to learn temporal graph representations. A Transformer encoder with a patching method is used to capture long-range dependencies across nodes. To preserve correlations between source and target nodes, DyGFormer integrates a Neighbor Co-occurrence Feature.
- **FreeDyG** (Tian et al., 2024a) delves the temporal graph modeling into the frequency domain and proposes a node interaction frequency encoding module that both effectively models the proportion of the re-occurred neighbors and the frequency of corresponding interactions of the node pair.

In addition to the above existing deep learning-based TGNNs, we also explore the performance and capabilities of the LLMs for TTAG modeling. We employ the widely adopted and well-performing LLM, DeepSeek-v2⁷ (Liu et al., 2024), an open-source project released by DeepSeek, Inc.⁸. DeepSeek-v2 is a strong, economical, and efficient mixture-of-experts language model. For comparison, we test its zero-shot and one-shot performance for temporal link prediction, which is denoted as LLM_{zero} and LLM_{one} , respectively. Similar to our temporal reasoning chain in Sec. 3.1, we design a task-specific prompt to call with LLMs. Specifically, given the historical interactions of two nodes, we prompt DeepSeek-v2 to directly predict whether these two nodes will interact at a specific future timestamp. The LLM’s response is confined to either “yes” (indicating an interaction exists) or “no” (indicating no interaction occurs). All requests with DeepSeek-v2 are conducted in a Language Model as a Service (LMaaS) compatible manner via its provided Application Programming Interface (API)⁹.

D.3. Implementation Details

Tasks and Metrics. We follow (Zhang et al., 2023) and conduct **temporal link prediction** under two settings: (i) transductive setting, which predicts links between nodes that have appeared during training; and (ii) inductive setting, where predictions are performed with unseen nodes. During training, we sample an equal number of negative destination nodes as described in Eq. 11. Inspired by (Huang et al., 2024), we employ Mean Reciprocal Rank (MRR) as the evaluation metric with 100 negative links per link during evaluation. Additionally, we further conduct the **node classification** task in a practical industrial application for financial risk management using the Industrial dataset from the e-commerce domain. The objective of this task is to predict whether a node is involved in fraudulent activity. Specifically, we follow (Zhang et al., 2023) and pass the learned representations through a two-layer MLP to get the probabilities of fraudulent activity for each node. We adopt the Area Under the Receiver Operating Characteristic Curve (AUC) as the evaluation metric for this task.

Model Configurations. For **training and evaluation**, we follow (Zhang et al., 2024a) and train all models for 50 epochs and adopt the early stopping strategy under patience of 5 with an evaluation interval of 5. The learning rate and the batch

⁷<https://github.com/deepseek-ai/DeepSeek-V2>

⁸<https://deepseek.com/>

⁹<https://api-docs.deepseek.com/zh-cn/>

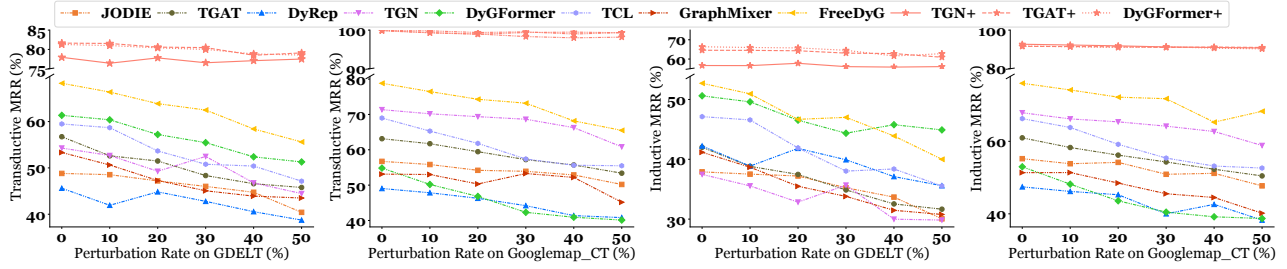


Figure 10. Robustness study for noise on GDELT and Googlemap_CT with different perturbation rates. (Supplementary results for Fig. 4.)

 Table 5. Ablation study for the raw texts and LLM-generated texts. **Semantic/Structural Encoding** refer to the encoding mechanisms that independently perform semantic/structural layers in Sec. 3.2; *imprv.* indicates the performance improvements of LLM-generated texts Text_{LLM} over the raw texts Text_{raw} . (Supplementary results for Tab. 2.)

	Datasets	Methods	Semantic Encoding			Structural Encoding			Structural-Structural Co-encoding		
			Text_{raw}	Text_{LLM}	<i>imprv.</i>	Text_{raw}	Text_{LLM}	<i>imprv.</i>	Text_{raw}	Text_{LLM} (ours)	<i>imprv.</i>
Transductive	GDELT	TGAT	49.64 ± 0.9	52.02 ± 8.8	↑ 2.38	56.73 ± 0.4	57.01 ± 0.3	↑ 0.28	58.29 ± 0.2	81.63 ± 1.7	↑ 23.34
		TGN	49.64 ± 0.9	52.02 ± 8.8	↑ 2.38	54.28 ± 1.6	55.58 ± 1.0	↑ 1.30	56.27 ± 1.2	77.95 ± 2.8	↑ 21.68
		DyGFormer	49.64 ± 0.9	52.02 ± 8.8	↑ 2.38	61.35 ± 0.3	62.54 ± 0.1	↑ 1.19	62.73 ± 0.5	81.28 ± 4.4	↑ 18.55
	Googlemap_CT	TGAT	47.03 ± 0.2	98.38 ± 0.4	↑ 51.35	63.13 ± 0.5	68.69 ± 0.1	↑ 5.56	65.46 ± 0.2	99.92 ± 0.0	↑ 34.46
		TGN	47.03 ± 0.2	98.38 ± 0.4	↑ 51.35	71.35 ± 0.5	81.60 ± 1.0	↑ 10.25	72.64 ± 0.8	99.92 ± 0.0	↑ 27.28
		DyGFormer	47.03 ± 0.2	98.38 ± 0.4	↑ 51.35	54.82 ± 2.7	61.76 ± 0.1	↑ 6.94	57.02 ± 0.4	99.82 ± 0.0	↑ 42.80
Industrial	TGAT	24.47 ± 0.5	73.15 ± 1.8	↑ 48.68	46.74 ± 3.9	53.33 ± 2.7	↑ 6.59	47.62 ± 2.0	86.97 ± 2.8	↑ 39.35	
	TGN	24.47 ± 0.5	73.15 ± 1.8	↑ 48.68	54.46 ± 3.0	53.20 ± 1.0	↓ 1.26	55.45 ± 0.5	94.26 ± 0.8	↑ 38.81	
	DyGFormer	24.47 ± 0.5	73.15 ± 1.8	↑ 48.68	74.45 ± 0.7	74.05 ± 0.4	↓ 0.40	75.23 ± 0.1	94.78 ± 1.4	↑ 19.55	
Inductive	GDELT	TGAT	27.98 ± 0.7	37.72 ± 9.5	↑ 9.74	42.01 ± 0.5	45.79 ± 0.4	↑ 3.78	41.02 ± 0.3	64.56 ± 1.8	↑ 23.54
		TGN	27.98 ± 0.7	37.72 ± 9.5	↑ 9.74	37.48 ± 2.8	34.61 ± 3.1	↓ 2.87	38.81 ± 1.0	56.65 ± 3.8	↑ 17.84
		DyGFormer	27.98 ± 0.7	37.72 ± 9.5	↑ 9.74	50.61 ± 0.2	52.33 ± 0.4	↑ 1.72	52.19 ± 0.3	66.37 ± 4.4	↑ 14.18
	Googlemap_CT	TGAT	44.43 ± 0.2	89.53 ± 0.7	↑ 45.10	60.96 ± 0.2	66.98 ± 0.2	↑ 6.02	62.17 ± 0.2	91.59 ± 0.0	↑ 29.42
		TGN	44.43 ± 0.2	89.53 ± 0.7	↑ 45.10	67.88 ± 0.2	78.08 ± 1.0	↑ 10.20	68.17 ± 0.2	92.68 ± 0.1	↑ 24.51
		DyGFormer	44.43 ± 0.2	89.53 ± 0.7	↑ 45.10	52.98 ± 2.5	59.67 ± 0.1	↑ 6.69	53.81 ± 0.6	91.74 ± 0.1	↑ 37.93
	Industrial	TGAT	20.71 ± 0.5	46.34 ± 2.3	↑ 25.63	30.04 ± 3.0	33.86 ± 1.2	↑ 3.82	34.19 ± 1.2	62.22 ± 2.1	↑ 28.03
		TGN	20.71 ± 0.5	46.34 ± 2.3	↑ 25.63	38.28 ± 4.1	34.41 ± 1.4	↓ 3.87	40.17 ± 2.0	83.23 ± 2.6	↑ 43.06
		DyGFormer	20.71 ± 0.5	46.34 ± 2.3	↑ 25.63	54.20 ± 0.4	54.18 ± 0.2	↓ 0.02	55.37 ± 2.7	82.30 ± 1.2	↑ 26.93

size across all models and datasets are set to 0.0001 and 256, respectively. We repeat the experiments for 3 runs with seeds ranging from 0 to 2 to ensure evaluation reliability and report the averaged performance with the corresponding standard deviations. All training is performed on a single server with 72 cores, 128GB memory, and four Nvidia Tesla V100 GPUs. As for **hyper-parameters**, the representation dimensions across all models and datasets are consistently set to 384, and the introduced hyper-parameter, maximum reasoning count m , is set to 8 for all datasets by default. Other hyper-parameters among both backbones and baselines follow the critical hyper-parameters in the widely-used library DyGLib¹⁰ (Yu et al., 2023), which has performed an exhaustive grid search to identify the optimal hyper-parameters across different models.

E. Related Work

Temporal Graph Neural Networks (TGNNs). Temporal graph neural networks (TGNNs) (Wen & Fang, 2022; Xiang et al., 2023; Tian et al., 2024a) are designed to generate node representations in temporal graphs, where they typically develop various structural encoding mechanisms to summarize the dynamic graph structures among neighborhoods of the target node (Goyal et al., 2020; Rossi et al., 2020b; Chang et al., 2020; Pareja et al., 2020; Wang et al., 2021d; Fan et al., 2021; Gao & Ribeiro, 2022; Zhang et al., 2023; Chen et al., 2024a; Zhang et al., 2024c). Based on how these mechanisms operate, existing TGNNs can be broadly categorized into two types: message-encoding TGNNs (ME-TGNNs) and walk-encoding TGNNs (WE-TGNNs). ME-TGNNs (Wang et al., 2021c;b; Alvarez-Rodriguez et al., 2021; Zhou et al., 2022; Luo & Li, 2022) capture changing graph structures via message passing mechanisms, where node representation is refined by aggregating messages from neighbors through various aggregation functions (Zhang et al., 2024b). In contrast, WE-TGNNs (Wang et al., 2021e; Souza et al., 2022) incorporate temporal structural information into node representations in a different

¹⁰<https://github.com/yule-BUAA/DyGLib>

way. They typically sample multiple temporal walks originating from the target node and encode these walks based on node occurrence information. Despite their success, above existing TGNNs focus solely on biased encoding mechanisms that prioritize topological information, neglecting the rich text semantics present in temporal text-attributed graphs (Zhang et al., 2024a). Instead, our model seamlessly integrates text semantics and graph structures, thereby effectively generating representations that are both context- and structural-aware.

Text-attributed Graphs (TAGs). Text-attributed graphs (TAGs) have been widely adopted in numerous real-world applications (Ren et al., 2024; Tan et al., 2024). To enable representation learning in such graphs, existing methods often combine graph learning approaches with language modeling techniques. Early works focus on integrating pre-trained language models (LMs) with graph neural networks (GNNs). Some of them (Zhao et al., 2022; Yasunaga et al., 2022) conduct cascaded architecture. They first use LMs to independently embed texts as node features, which are then fed into GNNs for representations. Unlike these pipelines, other methods (Yang et al., 2021; Zhang et al., 2022; Jin et al., 2023c;b;a; Zhu et al., 2024) adopt an iterative architecture to jointly detect both semantic and structural information. In recent years, the rising prominence of large language models (LLMs), such as DeepSeek-v2/3 (Liu et al., 2024), has underscored their exceptional potential to revolutionize TAG modeling (Zhu et al., 2024; Tian et al., 2024b; Tang et al., 2024). They typically harness the prompt response of LLMs as the external knowledge to fortify overall model performance, either for feature augmentation (He et al., 2023; Duan et al., 2024; He et al., 2024) or for structure refinement (Li et al., 2024; Fang et al., 2024). Unfortunately, all these methods overlook the potential temporal information inherent in graphs, limiting their applicability to TTAG modeling. Moreover, they cannot be directly applied to TTAGs, as TTAGs and TAGs differ technically. For instance, TTAGs involve a sequence of timestamped interactions with both node and edge attributes, while TAGs typically rely on adjacency matrices with only node attributes.

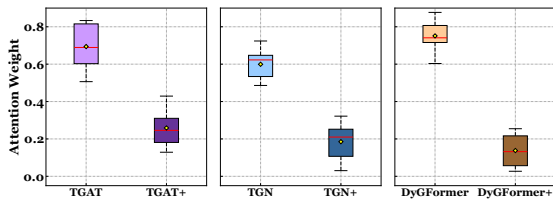
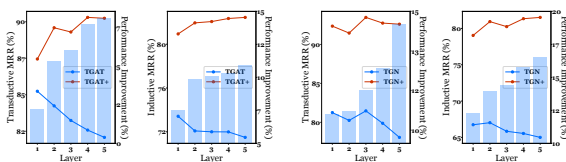


Figure 11. Attention weights from randomly selected nodes to their perturbed neighbors on Enron with the perturbation rate of 50%. (Supplementary results for Fig. 5.)



(a) TGAT model.

(b) TGN model.

Figure 12. Robustness study for encoding layers on ICEWS1819. (Supplementary results for Fig. 6.)

F. Cost Analysis for LLM Usage

As previously mentioned, we engage with the LLM, DeepSeek-v2, in a Language Model as a Service (LMaaS)-compatible manner with the provided API. In this section, we present a cost analysis for this operation.

Cost Statistics. DeepSeek-v2 is renowned for its exceptional performance and cost-efficiency, which provides an excellent balance between quality and affordability. Therefore, we select this model as the backbone of our Temporal Semantics Extractor to summarize the text semantics of the neighborhoods for target nodes at different timestamps. Here, we present the cost statistics for calling DeepSeek-v2 API across the four public datasets in Tab. 6 for reference. Additionally, we want to emphasize that the DeepSeek-v2 API imposes no theoretical rate limits. During practical implementation, we leverage

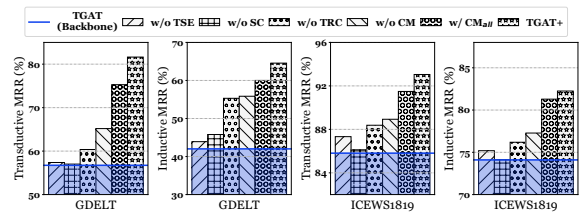
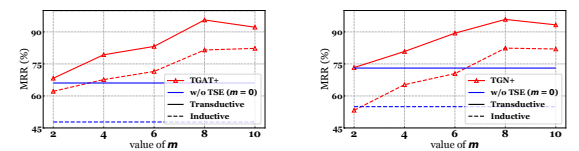


Figure 13. Ablation study for model components in boosted TGAT model. The results for TGAT backbone are included for reference. (Supplementary results for Fig. 7.)



(a) TGAT model.

(b) TGN model.

Figure 14. Parameter study with different maximum reasoning count m on Enron. The results for w/o TSE are shown for reference. (Supplementary results for Fig. 8.)

multithreading techniques to conduct multiple network requests simultaneously under 80 concurrent processes, enhancing program parallelism and optimizing response time consumption. As for the money cost, DeepSeek-v2 prices at \$0.00027 per 1,000 input tokens and \$0.0011 per 1,000 output tokens.

Table 6. Cost statistics of LLM usage.

Datasets	# Input Tokens	# Output Tokens	# Time Consumption (s)	# Money Cost (\$)
Enron	20,640,423	4,471,765	4,528	10.49
GDELT	4,194,490	1,049,842	4,145	2.29
ICEWS1819	21,844,799	5,410,145	6,517	11.85
Googlemap_CT	144,712,376	21,214,481	21,581	62.41

Efficiency and Reuse of LLM-generated Texts. It is important to highlight that we have implemented several strategies to enhance the efficiency of LLM utilization as follows: (i) Model Design. We introduce a maximum reasoning count m to constrain the number of reasoning steps for each node as described in Eq. 1. This design reduces the computational complexity of LLM calls from $\mathcal{O}(|\mathcal{E}|)$ to $\mathcal{O}(|\mathcal{V}|)$, where $|\mathcal{E}|$ and $|\mathcal{V}|$ represent the total number of edges and nodes respectively. (ii) API Interaction. We employ multithreading techniques for API access, substantially reducing the overall time consumption of LLM queries. (iii) Text Reusage. Our method requires only a single query to the LLM, with the summaries being stored for subsequent use. These LLM-generated texts can be reused for other tasks or integrated into other methods. We will make the LLM-generated texts publicly available if this paper can be accepted.

G. Prompt Template

In Sec. 3.1, we provide a simplified example of the prompts used to construct the temporal reasoning chain within our Temporal Semantics Extractor. Here, we present a complete example of the prompts applied to the Googlemap_CT dataset as depicted in Fig. 15. Only minor keyword adjustments are required for the prompts when applied to other datasets. Specifically, for the Enron dataset, the terms “item” and “review” are replaced with “user” and “email”. Similarly, for the GDELT and ICEWS1819 datasets, these terms are substituted with “entity” and “relation”. For the industrial datasets, “item” and “review” are replaced with “user” and “transaction”.

```
# Goal #: Summarize the historical reviews of user 'Maureen Sobel' at the current timestamp and provide your semantic understanding for them.
# Descriptions #: xxx
# Current timestamp #: 27639
# Recent reviews of user 'Maureen Sobel' #:
0. timestamp: 27630 | item: 'Name: xxx. Description: xxx' | review: 'Had my hair cut and permed by a very experienced and...'
1. timestamp: 27246 | item: 'Name: xxx. Description: xxx' | review: 'Always clean and monitored. Have a good selection of machines ...'
2. timestamp: 26880 | item: 'Name: xxx. Description: xxx' | review: 'Basic auto parts store with lackadaisical stereotype staff who ...'
3. ...
...
Provide the summary STRICTLY in this form: Summary: xxx.
```

Figure 15. An example of the prompt used in the Temporal Semantics Extractor to query the LLM on Googlemap_CT.

H. Detailed Information for Ablation Study

Ablation study for model components. We start the ablation study by evaluating the contributions of the key components of our model, including the Temporal Semantics Extractor (TSE) in Sec. 3.1, the Semantic-structural Co-encoder (SC) in Sec. 3.2, and the Cross-modal Mixer (CM) in Eq. 9. We remove each component individually, resulting in three variants: **w/o TSE**, **w/o SC**, and **w/o CM**. Moreover, we disrupt the Temporal Reasoning Chain constructed by the TSE component via scrambling the chronological order in $\hat{\mathcal{T}}_u$ among Eq. 1, which results in a variant named **w/o TRC**. Additionally, to validate the rationale behind the design of our Cross-modal Mixer, we present results where all semantic representations are indiscriminately mixed. This variant is referred to as **w/ CM_{all}**.

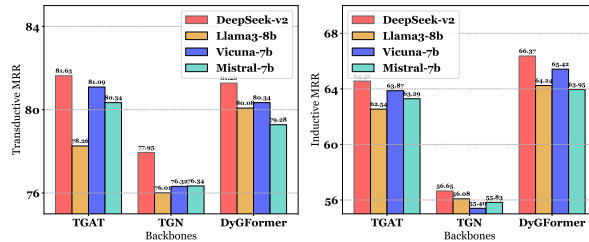


Figure 16. Ablation study for different LLMs on GDELT.

Ablation study for raw texts and LLM-generated texts. We then conduct an ablation study to compare the **raw texts** in TTAGs (*i.e.*, the original node or edge text attributes) with the **LLM-generated texts** (*i.e.*, neighborhood summaries produced by LLM-based Temporal Semantics Extractor). Experiments are performed using three encoding mechanisms, including the **semantic encoding** that performs semantic layers for semantic representations described in Sec. 3.2, the **structural encoding** that conducts semantic layers for structural representations described in Sec. 3.2, and the **semantic-structural co-encoding** that is used to generate final representations in CROSS. This leads to six combinations.

Ablation study for different LLMs. We further extend our ablation study with different LLMs. We conduct experiments using various LLMs with the GDELT dataset, including Llama3-8b (AI@Meta, 2024), Vicuna-7b (Chiang et al., 2023), and Mistral-7b (Jiang et al., 2023). Specifically, **Llama3-8b** is an auto-regressive language model with an improved transformer structure. Its tuned versions use supervised fine-tuning (SFT) and reinforcement learning with human feedback (RLHF) to align with human preferences for helpfulness and safety. **Vicuna-7b** is built on Llama 2 and fine-tuned using supervised instruction. Its training data comes from user-shared conversations found online. **Mistral-7b** uses grouped-query attention (GQA) for faster processing and sliding window attention (SWA) to handle long sequences more efficiently, reducing the cost of inference.

From the results in Fig. 16, we can find that our model consistently performs best, demonstrating the effectiveness of LLM DeepSeek-v2. Additionally, it is worth noting that the performance differences across various LLMs are relatively minimal. This demonstrates the robustness of CROSS’s framework.

I. Other Discussion

I.1. Complexity Analysis

Now, we provide a theoretical complexity analysis of the two main components of CROSS. Let $|\mathcal{V}|$ represent the number of nodes, D denote the average degree of the node, L indicate the number of encoding layers, and m depict the maximum reasoning count. To simplify the calculations, we assume that the input, hidden, and output dimensions are uniformly set to d . In the Temporal Semantics Extractor, we construct a temporal reasoning chain with a maximum reasoning count of m for each node, resulting in a computational complexity of $\mathcal{O}(m|\mathcal{V}|)$. For the Semantic-structural Co-encoder, we utilize various existing TGNN encoding blocks as the structural layers. Therefore, our complexity analysis focuses on the additional cost introduced by the semantic layers. As mentioned in Sec. 3.2, these layers employ a series of standard Transformer layers for each node, thus leading to a total complexity of $\mathcal{O}(L|\mathcal{V}|D^2d + L|\mathcal{V}|d)$.

I.2. Limitations

One potential limitation of CROSS is that we only focus on 1-hop historical interactions of a specific node as input to the LLM within our Temporal Semantics Extractor. While effective in many cases, this approach may be suboptimal for scenarios where high-order temporal semantics are critical. However, directly incorporating multi-hop textual neighborhoods into LLM could substantially escalate computational costs and dilute the model ability to capture relevant semantic information. Future work could explore innovative methods to efficiently and effectively capture nodes’ high-order semantics, unlocking further potential for improved TTAG modeling.

Another issue could be that LLM-generated texts do not always perform optimally under different encoding mechanisms. Although LLMs are renowned for their powerful text generation and understanding capabilities, it is crucial to explore effective encoding mechanisms that can fully maximize the potential of LLM-generated texts, such as the proposed Semantic-structural Co-encoder.